A Test of the Simulation of Tropical Convective Cloudiness by a Cloud-Resolving Model

MARIO A. LOPEZ, DENNIS L. HARTMANN, PETER N. BLOSSEY, ROBERT WOOD, CHRISTOPHER S. BRETHERTON, AND TERENCE L. KUBAR

Department of Atmospheric Sciences, University of Washington, Seattle, Washington

(Manuscript received 9 October 2007, in final form 4 November 2008)

ABSTRACT

A methodology is described for testing the simulation of tropical convective clouds by models through comparison with observations of clouds and precipitation from earth-orbiting satellites. Clouds are divided into categories that represent convective cores: moderately thick anvil clouds and thin high clouds. Fractional abundances of these clouds are computed as a function of rain rate. A three-dimensional model is forced with steady forcing characteristics of tropical Pacific convective regions, and the model clouds are compared with satellite observations for the same regions. The model produces a good simulation of the relationship between the precipitation rate and optically thick cold clouds that represent convective cores. The observations show large abundances of anvil cloud with a strong dependence on rain rate, but the model produces too little anvil cloud by a factor of about 4 and with a very weak dependence on the rain rate. The observations also show probability density functions for outgoing longwave radiation (OLR) and albedo with maxima that correspond to extended upper-level cold clouds, whereas the model does not. The sensitivity of the anvil cloud simulation to model parameters is explored using a two-dimensional model. Both cloud physical parameters and mean wind shear effects are investigated. The simulation of anvil cloud can be improved while maintaining a good simulation of optically thick cloud by adjusting the cloud physics parameters in the model to produce more ice cloud and less liquid water cloud.

1. Introduction

The role of clouds remains one of the primary uncertainties in projections of future climates (Bony et al. 2006; Solomon et al. 2007). Clouds and water vapor have a strong influence on the radiation budget of the earth, and it is unclear how cloud properties respond to global climate change. The tropics include half of the surface area of the earth, and account for much more than half of the earth's greenhouse effect. Tropical deep convection is important in setting the relationship between surface temperature and the radiation balance at the top of the atmosphere (Hartmann et al. 1992). High, cold clouds are particularly interesting because the extended upper-level clouds associated with tropical convection greatly influence both longwave emission and absorbed solar radiation, although their effect on the net energy balance is often much less than their individual effects on longwave and solar radiation (Hartmann et al. 2001).

Deep convective cores occupy a very small fraction of the tropical area. Extended upper-level clouds that vary from thick stratiform anvil clouds to thin cirrus clouds have more cloud mass and area than the cores of active deep convection and are much more important in the radiative balance of the earth. Anvil clouds associated with intense tropical convective systems are known to have long lifetimes and to cover large areas, accounting for a significant fraction of the precipitation produced by such systems (Leary and Houze 1980). Large mesoscale convective systems over the tropical western Pacific warm pool form long-lived structures called ''superclusters,'' which can extend for thousands of kilometers and last as long as 2 days (Nakazawa 1988; Mapes and Houze 1993; Chen et al. 1996).

The upper-level anvil clouds are important not only radiatively, but also in setting the structure of the vertical heating profile in the tropics. Precipitation from the anvils evaporates as it falls through the clear air below and this process makes the vertical profiles of heating and vertical velocity much more top heavy (Houze

Corresponding author address: Dennis L. Hartmann, Department of Atmospheric Sciences, University of Washington, P.O. Box 351640, Seattle, WA 98195-1640.
E-mail: dhartm@washington.edu

DOI: 10.1175/2008JCLI2272.1

1982). It is reasonable to suppose that the heating profile of organized convection in the tropics shapes the large-scale vertical velocity in the tropics (Mapes et al. 2006), and if so, this has significant implications for the large-scale flow (Hartmann et al. 1982; Lin et al. 2004; Schumacher et al. 2004). The vertical velocity profile is also very important in determining the gross moist stability and other diagnostics of the interaction of convection with large-scale thermodynamics (Back and Bretherton 2006). The interaction between organized deep convection and large-scale motion is a central issue in tropical meteorology.

Although some climate models have an upper-level ice cloud parameterization tied to the convection scheme and can produce reasonable simulations of upper-level clouds (Comstock and Jakob 2004), upper-level ice clouds are often deficient in amount or spatial structure (Li et al. 2005), and others show clear deficiencies related to the proper simulation of tropical anvil clouds (Ringer and Allan 2004). No global climate models currently have a tested parameterization for anvil cloud dynamics, although GCM parameterizations are beginning to consider more explicit incorporation of the effects of mesoscale circulations and anvil cloud formation (Donner et al. 2001). It has been proposed that a way forward is to use much greater spatial resolution, perhaps with cloud-resolving models (CRMs) embedded within a more coarsely gridded global climate model (Grabowski 2001; Randall et al. 2003a). In this manner the interactions between mesoscale circulations, cloud physics, and radiation may be incorporated explicitly in a global climate model for a computational cost that is less than a global cloud-resolving model. This is especially important in the tropics, where large-scale forcing of convection is less dominant than in midlatitudes, and self-organization of convection is critical (Su et al. 2000; Grabowski 2003c). Wu (2002) performed radiative-convective equilibrium calculations above a mixed layer SST model and showed a strong dependence of the equilibrium climate on the rate of ice sedimentation. An important step is to verify that CRMs of the type proposed for inclusion in climate models can simulate key processes realistically and produce realistic cloud properties.

CRMs are designed to simulate convection explicitly. They have much finer horizontal resolution than GCMs, with grid sizes typically 1–5 km compared with hundreds of kilometers in GCMs. At higher spatial resolution, the vertical motions of cloud-scale convective plumes are assumed to be resolved using the prognostic equations of motion, so a convective parameterization is not used. Cloud microphysical processes and subgrid turbulent transport must still be parameterized, however. CRMs can be used to compute radiative-convective equilibrium (Tompkins and Craig 1998), or they can be driven with specified large-scale dynamical forcing.

CRM validation methodologies have involved comparing the results of both CRMs and single column models (SCMs) to observations. Luo et al. (2005) demonstrate that the University of California at Los Angeles–Colorado State University (UCLA–CSU) CRM produces more realistic cirrus cloud properties than the SCM version of the Global Forecast System model. Using a variety of both CRMs and SCMs to simulate ARM observations, Randall et al. (2003b) demonstrate that CRMs produce smaller biases in vertical profiles of water vapor, temperature, and cloud occurrence than SCMs. Because CRMs perform better than SCMs in radiative convective equilibrium simulations, it has been proposed that GCM simulations may improve if their convective parameterization schemes are replaced with a CRM embedded in each grid cell. These schemes have shown promise in helping models produce realistic Madden–Julian oscillations (Grabowski 2003b; Randall et al. 2003b). Ovtchinnikov et al. (2006) show that a GCM using an embedded CRM convective scheme produces too little high cloud compared to observations, however. Wyant et al. (2006a) compare clouds produced by a GCM using superparameterization to International Satellite Cloud Climatology Project (ISCCP) data, showing that in different dynamical regimes the model tends to either overpredict or underpredict cloud fraction. Both GCMs with embedded CRMs and global cloud-resolving GCMs are beginning to be used to evaluate climate sensitivity (Miura et al. 2005; Wyant et al. 2006b).

More effort should be devoted to methodologies that compare CRMs with observational data directly, especially their ability to simulate realistic clouds and their relation to the top-of-atmosphere (TOA) radiation balance. Wu et al. (1999) performed a 39-day simulation of the Tropical Ocean and Global Atmosphere Coupled Ocean–Atmosphere Response Experiment (TOGA COARE) period using a 2D model, and emphasized the importance of the cloud physics parameterizations in simulating observations of surface radiative fluxes. Comparing the Advanced Regional Prediction System/Langley Research Center CRM to satellite observations, Eitzen and Xu (2005) showed differences in probability density functions (PDFs) of albedo and outgoing longwave radiation (OLR) between large cloud objects in the model and in observations. Luo et al. (2007) found that a CRM intended for use as part of a superparameterization tended to underestimate higher albedos. Blossey et al. (2007) compared the System for Atmospheric Modeling (SAM) to Kwajalein Experiment (KWAJEX) observations, and showed persistent

biases in albedo and OLR due to an insufficient amount of high clouds during periods of low to moderate precipitation. Zhou et al. (2007) compared a 3D model with 2-km horizontal grid spacing to observations from satellites and found that the convection tended to form in dense packets with less than the observed amount of anvil cloud.

Here we demonstrate a method of bringing satellite data to bear on testing the simulation of tropical convective cloud structure by a cloud-resolving model. This comparison focuses on the necessity of properly simulating the distribution of optical depth in cold clouds. Hartmann et al. (2001) have shown that the distribution of optical depth within tropical convective systems is critical to determining the net effect of these clouds on the earth's energy budget. We compare the distributions of high clouds produced by the SAM model run in a tropical domain with distributions observed from space by the Moderate Resolution Imaging Spectroradiometer (MODIS) instrument, using the Advanced Microwave Scanning Radiometer (AMSR) instrument to sort the data by rain rate. Particular attention will be given to simulating the correct distribution of optical depth for cold clouds. PDFs and domain averages of albedo and OLR are also examined to help quantify the relationship between clouds and the TOA energy budget in the model. Section 2 describes the observational methodology. Sections 3 and 4 present three-dimensional (3D) simulations and results. Section 5 introduces the two-dimensional (2D) methodology that is used to test how changes to the model may affect anvil cloud amount, and section 6 details these 2D experiments. Finally, section 7 offers a discussion and the conclusions.

2. Observational methodology

The goal is to compare cloud-resolving model simulations of tropical convection with satellite observations to test the validity of the model. The observational methodology follows that of Kubar et al. (2007, hereafter KHW), in which coincident measurements of precipitation from the AMSR (Wilheit et al. 2003) and cloud optical depth and cloud-top temperature measurements from MODIS (Platnick et al. 2003) are used to show the relationship of cloud properties to precipitation rate in the tropics. We use the version 5 AMSR rain-rate data (Remote Sensing Systems 2006), which are available daily for $0.25° \times 0.25°$ region. The validation of AMSR precipitation estimates is ongoing, but previous studies of microwave remote sensing of precipitation suggest biases against independent measurements in oceanic areas of 10%–20% (Kummerow et al. 2001; DeMoss and Bowman 2007). Since our analysis technique involves averages of large samples, it is the bias that is of most concern. MODIS joint level 2 cloud data are used, which have a resolution of 5 km. Both these datasets are averaged up to $1° \times 1°$ resolution grids and averages are taken over three days to form the basic dataset. This averaging in space and time reduces the effect of instantaneous sampling variations of the two datasets, but still captures a wide range of average rain rates and associated cloud properties that can be compared with the variability of the models. The results are not sensitive to the details of the averaging (KHW). All observations are made at 1330 LT. The diurnal variation of tropical convection over the oceans inferred from satellite data is small compared to the total variability (Hendon and Woodberry 1993). More details of the data analysis can be found in KHW.

KHW consider clouds with tops colder than 245 K and divide them into groups according to the optical depth. This temperature corresponds to a relative minimum in the distribution of cloud-top temperature measured by MODIS. Two optical depth cutoffs were chosen. An optical depth (τ) of four approximately separates thin clouds with a positive net cloud radiative forcing from thicker clouds that cause a net reduction in the radiation balance at the top of the atmosphere. KHW defined cold clouds with $\tau < 4$ as thin clouds, cold clouds with $4 < \tau < 32$ as anvil clouds, and cold clouds with $\tau > 32$ as thick clouds. KHW found that thick clouds thus defined have a relationship with AMSR precipitation that is the same in the east Pacific (EP) and west Pacific (WP), while anvil and thin clouds have a different relationship with precipitation in the EP and WP. High optical depth clouds ($\tau > 32$) are relatively rare in the MODIS observations, but they are an excellent marker for the deep convective cores that initiate much of the precipitation. Here we use these same definitions of thin, anvil, and thick clouds to test the relationship of clouds to precipitation in a cloud-resolving model. The partitioning of cloud types by optical depth is a simplification of previous ISCCP categorizations (Chen et al. 2000; Rossow et al. 2005), but the separation into warming, cooling, and heavily precipitating cold clouds is a physically motivated and objective basis for comparing models with data in a way that relates cloud morphology to cloud-radiative effects.

Rather than using cloud properties and precipitation derived from satellite observations, one could use the model data to generate expected MODIS and AMSR radiances and compare those, as is done with satellite profiling radiances in modern data assimilation schemes. Such an analysis is well beyond the scope of the current effort, and we choose rather to compare in situ state

variables from the model with state variables inferred from satellite observations.

3. Three-dimensional modeling methodology

We employ the System for Atmospheric Modeling (SAM) version 6.3, a three-dimensional CRM developed at CSU (Khairoutdinov and Randall 2003). The 3D SAM simulations are set up in a similar manner to those in Blossey et al. (2007). We use a horizontal domain of 256 by 256 km with 1-km grid size. The model has 64 levels in the vertical. Spacing between levels varies from 75 m at the surface to 400 m through most of the troposphere and finally 1 km in the ''sponge region'' (top 30% of domain). To represent near-equatorial conditions, the Coriolis parameter is set to zero. The model does not use a planetary boundary layer scheme apart from smaller vertical grid spacing near the surface and surface flux parameterizations for momentum, heat, and moisture. SST is specified. The model utilizes a Smagorinsky scheme for subgrid-scale turbulent transport and the radiation scheme from the Community Atmosphere Model, version 3 (CAM3). Insolation is constant with the diurnal average zenith angle and irradiance. A nominal 6-s time step is used. Radiation is computed every 6 min.

The prognostic thermodynamic variables in SAM are nonprecipitating water, precipitating water, and liquid–ice static energy. Nonprecipitating water includes water vapor, cloud liquid, and cloud ice, while precipitating water includes rain, snow, and graupel. Partitioning between hydrometeor species is based on temperature. Supersaturation of water vapor is not allowed. In the CAM3 radiation scheme, water vapor, cloud liquid, and cloud ice are all radiatively active, but precipitating hydrometeors are not. Luo et al. (2003) have shown that the absorption of radiation by snow can be important, but in our model the mass of snow is less than that of cloud ice, even in the base case in which ice falls relatively quickly, and because the particle radius of snow is so much larger than ice, the error in the optical depth caused by neglecting snow is generally less than 10% in these experiments. For the base case, the default one-moment bulk microphysical parameterization of SAM is used (see appendix A of Khairoutdinov and Randall 2003), except that cloud ice fall speed is calculated as a function of ice water content following Heymsfield (2003), replacing the default parameterization in which cloud ice fall speed is fixed at a constant value of 40 cm s^{-1}.

Profiles of zonal wind are specified, and domain-mean zonal winds are nudged to these prescribed values on a 2-h time scale. To test the influence of wind shear, three mean wind profiles are considered. In the base case the wind decreases from 5 m s^{-1} at the surface to zero at the tropopause (shear 5). Additional experiments are performed in which the mean wind varies from 5 m s^{-1} at the surface to -15 m s^{-1} at the tropopause, resulting in a quadrupling of the wind shear (shear 20). The latter case is a good approximation to the maximum climatological wind shear in the tropics. Finally, the wind profile from TOGA COARE, shown in Wu (2002) is used (shear TC). This profile has a low-level wind maximum, relatively weak shear in the midtroposphere, and strong shear of about 15 m s^{-1} between 10 km and the tropopause. The surface meridional wind in this profile is modified to bring the surface wind speed to 5 m s^{-1} as in the other two cases, in order to eliminate a change in surface fluxes associated with the mean surface wind speed.

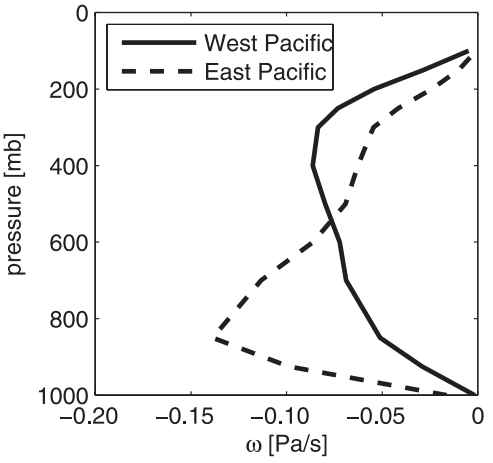

FIG. 1. Profiles of vertical motion in WP and EP regions used to compute thermal forcing for the 3D simulations.

We wish to compare satellite observations with cloud-resolving model simulations. In order for this to be useful, we must set up the model in such a way that we might expect it to produce the observed cloud statistics. Convectively active regions of the tropical (EP; 7.5°–10°N, 140°–120°W) and WP (5°–7.5°N, 140°–160°E) are selected. Large-scale forcing is applied to the simulation by imposing the temperature and moisture forcing consistent with vertical advection of the large-scale vertical velocity profiles derived by Back and Bretherton (2006) from reanalysis data (Fig. 1). Qualitatively, these profiles are described as ''bottom heavy'' in the EP and ''top heavy'' in the WP. Each profile has been normalized in amplitude to produce a domain-mean rainfall rate of approximately 15 mm day^{-1}. Differences between the clouds in the simulations for the EP and WP regions are thus due to the profile shape, not the overall domain-mean intensity of convection. This rain rate is higher than observed in order to produce relatively

vigorous convection with steady forcing. We also perform simulations with the forcing reduced so that the precipitation is close to that observed by AMSR. SST is fixed at 302.49 K in both simulations to assure that differences between the two simulations are a result of the imposed vertical motion profiles, rather than differences in SST. We have done additional simulations in which the SSTs are closer to their observed values in each region, but the radiative convective equilibrium (RCE) cloud distributions are not very sensitive to the uniform variations in the SST of 1° or 2°C (Lau et al. 1994).

The 3D simulations are run for a total of 10 days, after having been run on a smaller 64 km by 64 km domain for 50 days to a state of RCE. Instantaneous fields are output every hour. The final 9 days when the 256 × 256 km model has equilibrated are used to gather the cloud and precipitation statistics for comparison with the observations. Because thin, anvil, and thick cloud fractions are not model output variables, they are calculated from the instantaneous model data, using a column-by-column algorithm. In each layer of every column, visible optical depth is calculated using the liquid/ice water path and the effective radius:

$$\tau_{\text{layer}} = \frac{3}{2}\frac{\text{LWP}}{r_{\text{el}}} + \frac{3}{2}\frac{\text{IWP}}{r_{\text{ei}}}, \qquad (1)$$

where liquid water path (LWP) and ice water path (IWP) are in g m^{-2}, and r_{el} and r_{ei} are the effective radii for liquid and ice clouds in microns, respectively. The effective radius for cloud liquid water is 14 μm. For cloud ice, effective radius varies from ~6 μm at temperatures below 180 K to ~250 μm at temperatures above 274 K, using a lookup table. These are the same specifications used in the radiative transfer model in the simulations. Total column visible optical depth is then calculated as the cumulative sum of the optical depth in every layer of the column.

Because we desire to determine cloud-top temperature using a technique similar to that of the satellite observations with which we will compare the model, cloud-top temperature, T_c, for the column is determined as the temperature at the top of the layer where cumulative optical depth from TOA exceeds 0.1, which is intended to mimic the detection threshold for MODIS. Clouds are classified as high, if $T_c < 245$ K. Cloud fractions for the cold cloud types defined by KHW are determined for blocks of 64 km by 64 km, which is approximately the size of the blocks in the satellite data.

We examine high cloud fraction as a function of rain rate. Rain rate is directly related to the latent heating term that drives the tropical circulation, and the relationship between rain rate and cloud amount is a fundamental quantity of importance for climate. For each block, the mean rain rate is obtained by averaging the surface rain rate of all the columns within the block. Using instantaneous hourly output fields, an aggregate of cloud fractions and mean rain rates is formed. Percentiles of rain rates are calculated from the mean rain rates, ignoring mean rain rates less than 0.1 mm day^{-1} so that the percentiles will better resolve the larger rain rates. We next bin cloud fraction by percentile of rain rate to obtain a relationship between average cloud fraction and rain rate as in KHW.

4. Three-dimensional results

Figure 2 shows the cloud amounts for the EP and WP regions as a function of rain rate for both the 3D model simulations and for the satellite observations. The baseline 2D case is also shown and will be described later. The bottom panel shows the relationship of thick cloud ($T_c < 245$ K, $\tau > 32$) fraction to precipitation rate. The model and the observations fall nearly on the same lines in both the EP and WP regions. The middle panel shows the relationship of anvil cloud fraction ($T_c < 245$ K, $4 < \tau < 32$) to precipitation rate. In this case the model shows far too little anvil cloud and the anvil cloud amount does not increase with the precipitation rate as observed. The top panel shows the thin cloud ($T_c < 245$ K, $\tau < 4$) fraction as a function of the rain rate. The thin cloud fractions are more similar those observed, the weak dependence of the thin cloud on the precipitation rate is simulated, and the much larger thin cloud amount in the WP than the EP is also simulated. These results suggest that the thin clouds in both the model and the observations are not uniquely related to the amount of anvil cloud. Animations of the model simulation suggest that the thin cloud is not connected directly to the anvil cloud, but rather seems to be a result of the uniform cooling imposed at high levels (Fig. 1). Simulations performed for the base case conditions with the shear increased by a factor of 4–20 m s^{-1} between the surface and the tropopause do not produce significantly better agreement with observations than that shown in Fig. 1. Later we will show that when the cloud physics parameterization is modified to produce more ice, the model produces a sensitivity of clouds to shear that is in agreement with observations.

Thin cloud fraction is somewhat independent of rain rate in both the EP and WP simulations, but a decrease in thin cloud fraction occurs at the highest rain rates. This decrease at high rain rates is due to convective cores and anvils being the dominant cloud species in

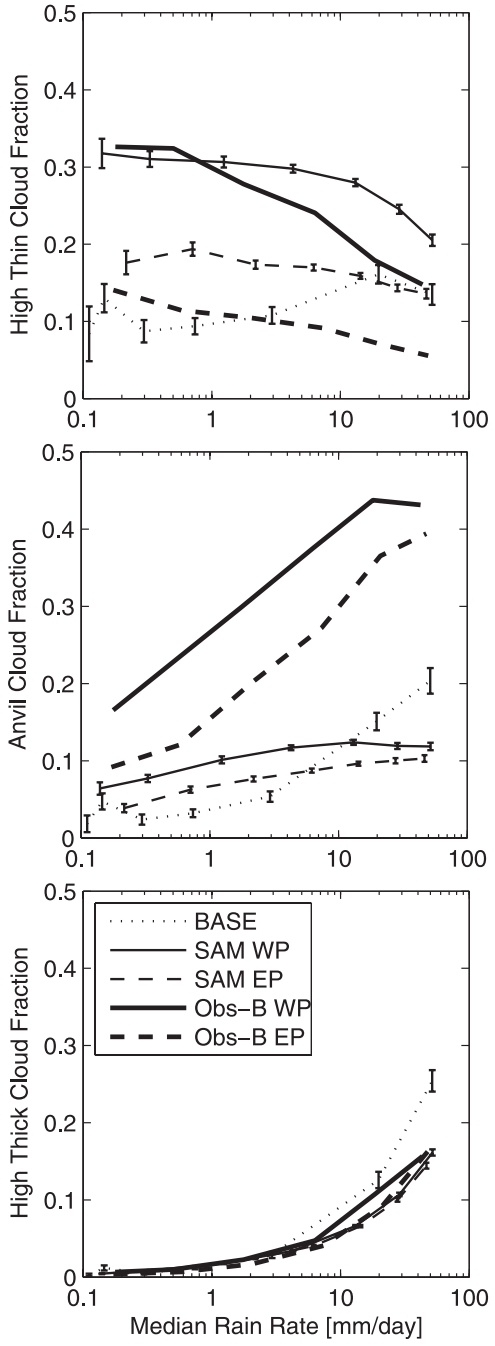

FIG. 2. Average cloud fraction as a function of precipitation rate percentiles for EP (dashed) and WP (solid) regions from observations (thick lines), from the 3D SAM model for the EP and WP regions (thin lines), and from the BASE simulation of the 2D SAM model (dotted thin line). (top) The fractional coverage of optically thin, cold cloud ($T < 245$ K, $\tau < 4$), (middle) fractional coverage of anvil clouds ($T < 245$ K, $4 < \tau < 32$), and (bottom) fractional coverage of thick cloud ($T < 245$ K, $\tau > 32$).

places where precipitation is most intense, thus decreasing the space available within the $1° \times 1°$ box for the thin cloud.

Because the cloud fraction versus rain rate composites only convey information about cloud amount in places where precipitation is occurring, it is possible that our methodology fails to detect some anvil clouds, if they spread to regions where precipitation is extremely light (less that 0.1 mm day^{-1}). To eliminate this as a possibility, we examine domain average cloud fraction.

Table 1 shows domain average comparisons between the SAM model simulation and the satellite observations for the EP and WP regions derived from MODIS temperature–optical depth histograms. Although the rain rate in these simulations is greater than that in the observations, the anvil cloud fraction is much smaller than observed, confirming that the 3D simulations do not produce enough anvil cloud. Domain average high thick cloud fraction is also less than expected, given the difference in precipitation rates. The model produces a reasonable amount of thick cloud per unit of precipitation when divided into a precipitation spectrum, but the scale in Fig. 2 is logarithmic and much of the precipitation comes in a relatively small number of very intense events. Domain-average high thin cloud fraction is slightly higher than observations in the EP and nearly agrees with observations in the WP. Although the rain rate composites suggest that the model overproduces high thin cloud in the WP, the unexpected agreement with observations in Table 1 may indicate that high thin clouds in the WP are abundant in nonraining regions, perhaps sustained by gravity waves or the mean rising motion in the upper troposphere. Because the domain-average rain rate in the simulations is significantly larger than the AMSR observations, the amount of cold cloud per unit of precipitation in the model is very low compared to AMSR/MODIS observations, especially for clouds with intermediate optical depths. Table 1 shows that the anvil to thick cloud fraction in the observations is 5.2–6.6, but in the model it is 1.4–1.8.

Table 1 shows large biases in the domain-mean albedo, with the model albedo around 0.25 and the observed albedo nearly 0.4 in both regions. The model OLR is too high by 20 W m^{-2} in the EP and nearly 40 W m^{-2} too high in the WP. The model does show a higher OLR in the EP by about 20 W m^{-2}, compared to the observed EP − WP difference of 37 W m^{-2}. The OLR discrepancy is fractionally less than the albedo discrepancy because the model produces high, thin clouds in reasonable amounts, but far too little cloud with intermediate optical depths (anvil clouds). The thin clouds reduce the OLR, but have little effect on the albedo, for which the anvil clouds are very important.

TABLE 1. Domain averages from observations and SAM for the WP and EP.

	Obs-B WP	SAM WP	Obs-B EP	SAM EP
Rain rate (mm day^{-1})	8.2	14.7	8.9	15. 0
High thin cloud fraction	0.29	0.28	0.10	0.16
Anvil cloud fraction	0.31	0.11	0.23	0.09
High thick cloud fraction	0.05	0.06	0.04	0.06
Anvil to high thick ratio	6.6	1.8	5.2	1.4
Albedo	0.38	0.25	0.39	0.26
OLR (W m^{-2})	183	223	220	243

To further investigate how the lack of anvil clouds significantly affects the TOA energy budget, we examine PDFs of albedo and OLR. The PDFs are constructed from values of albedo and OLR at every point in the domain of the model as well as in the corresponding observational domain. To construct PDFs from the observations, the radiative transfer model of Fu and Liou (1993) is used to calculate albedo and OLR in the domain of the observations, based upon the MODIS observed cloud property histogram. The cloud properties used in the radiative transfer calculations are based upon pixel level MODIS data (5 km $\times$ 5 km), so that they can be directly comparable to the gridpoint level PDFs obtained from the model. Temperature and humidity profiles from the Atmospheric Infrared Sounder (AIRS) version 2 data from January 2003 to December 2005 are used in the calculations (Aumann et al. 2003).

In the observations, the PDF of albedo has two modes (Fig. 3). The first mode, centered near 0.1, corresponds to nearly clear skies. A second weak peak appears around 0.7, corresponding to optically thick clouds that are tropical anvil cloud structures and associated convective cores. In the simulations, clear skies occur more frequently, the PDF of albedo decays rapidly toward higher albedos, and the high albedo peak is absent. The model PDFs of OLR show discrepancies that are consistent with those of the albedo (Fig. 4). Observations show one peak at high OLR corresponding to clear skies and another peak at about 120 W m^{-2}, corresponding to the modal anvil cloud-top temperature. The model OLR PDF has a broad peak near the clear-sky value and does not show the observed peak at low OLR values that is associated with anvil clouds. The clear-sky peak in the model also occurs at a lower value of OLR than the PDF calculated from the MODIS–AIRS data. This may be associated with the strong thermal forcing of the model and the correspondingly moist upper troposphere in the simulations.

In the next section we will explore variations in cloud physics parameters within the context of a 2D model. We will see that the simulation of anvil cloud as diagnosed by Fig. 1 can be improved by increasing the amount of ice cloud while simultaneously decreasing the amount of liquid cloud.

5. Two-dimensional mock Walker simulations

The methodology we have used to test the 3D simulations can also be applied in a 2D context. In contrast to the 3D experiments, in the 2D runs the mean vertical velocity is determined internally to the model at all locations. Since we find similar deficiencies in anvil cloud simulation in the 2D and 3D simulations, this deficiency of the model is very robust to changes in the model setup. Two-dimensional simulations require less computer resources, and thereby allow easier testing of sensitivity to model parameters.

We begin by examining the base case (BASE), in a 2D SAM simulation like that described in Bretherton et al. (2006), which uses a horizontal domain size and a grid resolution of 4096 and 2 km, respectively. SST is fixed as a sinusoidal function of distance, creating a warm pool in the center of the domain with a maximum temperature of 301 K and a minimum temperature of 297 K. The atmosphere organizes into an overturning circulation with convection and upward motion mainly confined to the warm water (Grabowski et al. 2000; Bretherton et al. 2006). Vertical resolution and the parameterizations for microphysics, radiation, and subgrid turbulent transport remain the same as in the 3D runs. Although we do not apply large-scale forcing to the atmosphere directly, a large-scale circulation develops in response to the imposed SST gradient, allowing us to examine how high cloud properties depend upon surface precipitation rate in a less constrained environment than was used for the 3D simulations. In the BASE case domain-mean winds are nudged to zero on a 2-h time scale to prevent the development of mean shear unrelated to the Walker circulation. We also conduct simulations with domain-mean winds nudged to linear shears of 5 and 20 m s^{-1} as described for the 3D model.

The 2D model is run for a total of 50 days and results are saved every 3 h for the last 20 days of the integration. The same column-by-column algorithm from the

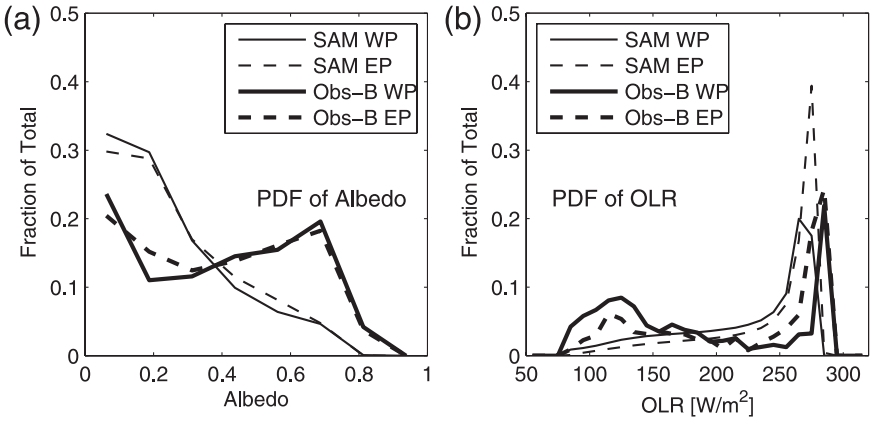

FIG. 3. PDF of (a) albedo and (b) OLR for the observations and for the 3D simulations for the EP and WP regions. Line conventions as in Fig. 2.

3D runs is used to determine the abundance of thin, anvil, and thick clouds. A larger horizontal averaging block size of 128 km is used for the 2D model in order to provide better sampling, and averages are taken over three adjacent time samples.

BASE has too little anvil cloud amount per unit of precipitation to roughly the same degree as the 3D runs (dotted line in Fig. 2), and the ratio of anvil cloud to thick cloud in BASE is 1.4, very similar to the 3D results, and far less than observed. Anvil cloud fraction seems to be more strongly dependent on rain rate than in the 3D runs, however, and anvil cloud fraction approaches 20% at the highest rain rate, compared to 40% in the observations. The thick cloud amount increases more quickly with rain rate than observed, however.

6. Parameter variations in 2D mock Walker simulation

Because BASE underproduces anvil cloud by roughly the same degree as the 3D runs, we use the mock Walker simulation as a tool for testing the sensitivity of anvil cloud in SAM to adjustments to the physics and resolution of the model. In this spirit, a suite of 2D mock Walker simulation experiments is performed using different adjustments to BASE, involving microphysics, resolution, domain size, and wind shear. The 2D experiments are summarized in Table 2. Microphysics experiments include reduction of cloud ice fall speed, decreased and increased rates of autoconversion and accretion, and elimination of graupel formation. In horizontal resolution experiments, resolution is increased from the default value of 2 km to 1 and 0.5 km. Vertical resolution experiments use an increased number of levels in the ice cloud layer. Experiments are also conducted with the domain size doubled to 8192 km, twice as large as in BASE. In these experiments the variation in SST has the same magnitude, but occurs over a larger domain.

a. Spatial resolution

Spatial resolution of the model may affect the physical processes important to anvil cloud formation. To investigate whether finer horizontal grid size than the default 2 km may increase anvil amount, we perform experiments that use horizontal grid sizes of 1 and 0.5 km, respectively. Also, it is useful to investigate the sensitivity of anvil cloud amount to changes in the vertical resolution of SAM. The VERTRES run increases vertical resolution by using 200 m spacing between levels throughout the ice cloud layer.

The experiments with higher horizontal and vertical resolution do not significantly affect the relationship between anvil cloud fraction and rain rate, or any of the cloud amounts (not shown). Pauluis and Garner (2006) found that increases in CRM horizontal resolution finer than 4 km do not affect the amount of simulated high cloud.

b. Domain size

A larger domain contains a more realistic SST gradient and gives convection more space to organize. The BIG run doubles the size of the horizontal domain to 8192 km, creating a warm pool twice as large as the one that exists when using the default domain size. Maximum and minimum SSTs and horizontal and vertical resolutions remain at their values used in BASE. The larger horizontal domain in BIG does not change anvil cloud amount significantly (not shown). A series of experiments was performed with microphysical changes with the doubled domain, but these results are consistent with the microphysical testing described below and will not be discussed.

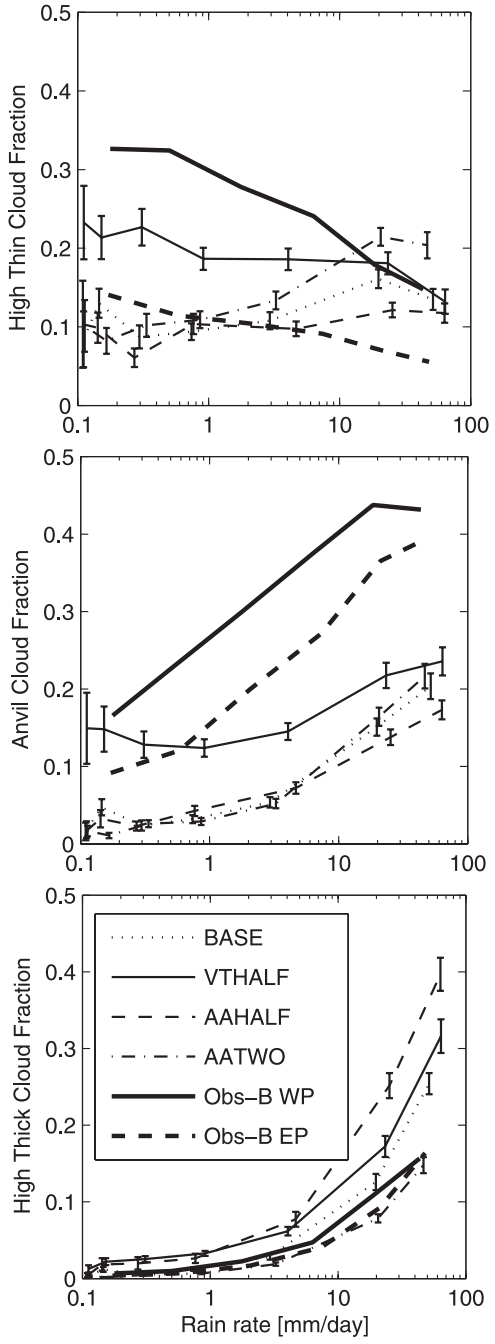

FIG. 4. As in Fig. 2, but the thin lines are for the 2D simulations BASE, VTHALF, AAHALF, and AATWO. Heavy lines again represent observations for the EP and WP.

c. Microphysics

Changes to microphysics can increase anvil cloud amount, because microphysical processes play a critical role in determining the amount of ice in the atmosphere. Krueger et al. (1995) used microphysical adjustments to increase the extent and ice water content of tropical anvil clouds in a CRM, by making changes to the parameterizations of cloud ice growth, snow formation, and graupel. Also, microphysical processes may affect atmospheric circulation. Fu et al. (1995) showed how interactive radiation affects simulated anvil cloud circulations and feeds back to the anvil cloud lifetime. By removing cold cloud processes from a 2D CRM, Grabowski (2003a,c) showed that in the warm-rain-only version of the model the mesoscale convective systems have a shorter life cycle and reduced stratiform component. In addition to direct effects on cloud formation and dissipation, cloud ice microphysics play an important role in determining mesoscale circulations that may be important to the dynamics of anvil clouds.

1) CLOUD ICE FALL SPEED

In the microphysical parameterizations of SAM, cloud ice is allowed to fall slowly, although it is considered to be a nonprecipitating hydrometeor species. We expect that anvil cloud amount will increase if cloud ice fall speed is reduced. In the BASE simulations cloud ice fall speed is parameterized as a function of ice water content, following Heymsfield (2003):

$$v_{t_{\rm ice}} = 165(\rm IWC)^{0.24}, \qquad (2)$$

with $v_{t_{\rm ice}}$ in cm s^{-1} and IWC in g m^{-3}. In the VTHALF run, the cloud ice fall speed computed in the preceding formula is multiplied by one-half.

VTHALF fails to improve the relationship between anvil cloud fraction and rain rate (Fig. 4). Although anvil cloud fraction increases noticeably, it becomes nearly independent of rain rate and is less than half the observed amount at the highest rain rates. Moreover, thick cloud fractions also increase in VTHALF, so that decreasing the ice fall speed increases the fractional coverage of all cloud types and does not improve the ratio of anvil cloud to thick cloud.

2) AUTOCONVERSION AND ACCRETION

The rate of autoconversion determines how quickly cloud liquid or ice is converted to precipitation by coalescence or aggregation, respectively. By reducing this rate, the onset of precipitation may be delayed, potentially prolonging cloud lifetime. The accretion rate controls the growth of precipitating condensate through the collection of nonprecipitating condensate. To examine the effect of changing the rates of autoconversion and accretion, the AAHALF, AATWO, and AATEN runs multiply the default rates of autoconversion and accretion for both liquid and ice by factors of 0.5, 2, and 10, respectively.

These experiments have little effect on anvil clouds. The relationship between anvil fraction and rain rate in

TABLE 2. Descriptions of 2D experiments. All changes are relative to BASE.

Run	Description
BASE	Default 2D simulation (see text)
VTHALF	Reduce cloud ice fall speed by half
AAHALF	Decrease rates of autoconversion and accretion for liquid and ice by half
AATWO	Increase rates of autoconversion and accretion for liquid and ice by factor of 2
AATEN	Increase rates of autoconversion and accretion for liquid and ice by factor of 10
HALFICE	Decrease rates of autoconversion and accretion for ice only by factor of 2
TWOICE	Increase rates of autoconversion and accretion for ice only by factor of 2
NOGRAU	Eliminate graupel as a hydrometeor species
HORRES 1	Increase horizontal resolution to 1 km
HORRES 0.5	Increase horizontal resolution to 0.5 km
VERTRES	Use 200-m horizontal resolution throughout the ice cloud layer
BIG	Double size of horizontal domain to 8192 km
NOSED	No ice sedimentation, lower ice autoconversion threshold by factor of 100
NOSEDAALIQ5	No ice sedimentation, lower ice autoconversion threshold by factor of 100; increase autoconversion and accretion rates for liquid water by a factor of 5
W30AALIQ2	Constant ice sedimentation of 30cm/s, increase autoconversion and accretion rates for liquid water by a factor of 2
SHEAR-5, SHEAR-20	Winds start at 5 m s^{-1} at the surface and then decrease linearly with height to zero (SHEAR 5) or -15 m s^{-1} (SHEAR 20) at the tropopause
SHEAR-TC	Mean wind profile from TOGA COARE as shown in Wu (2002)

AAHALF and AATWO is nearly identical to the relationship found in BASE (Fig. 4). AATEN is very similar to AATWO and is not shown. Interestingly, increasing the autoconversion rates as in AATWO reduces the thick cloud fractions so that they compare better with observations at all rain rates than BASE. Increased rates of autoconversion and accretion in AATWO increase precipitation efficiency in convective cores. As a result, high thick cloud fraction decreases because cloud liquid water below the freezing level is rained out more readily. Consistent with this, AAHALF noticeably overproduces high thick clouds, a bias that becomes quite large at rain rates greater than 10 mm day^{-1}.

We also experimented with changing the autoconversion and accretion rates for ice only. The results of these experiments are indistinguishable from BASE, so we conclude that the response of high cloud fraction in AAHALF and AATEN is mostly due to changes in the liquid autoconversion and accretion rates. Note that while we define high clouds by their cloud-top temperature, their albedos are affected by the water and ice content over a deep layer.

3) GRAUPEL

NOGRAU eliminates the formation of graupel as a precipitating species, but does not improve the relationship between anvil cloud fraction and rain rate (not shown). It is somewhat surprising that high thick cloud fraction remains similar to BASE, because the lack of graupel suggests an increase in the amount of cloud liquid water inside convective cores. Any changes in cloud water produced by the elimination of graupel seem to be offset by the other microphysical processes in the model.

4) COMBINATIONS OF CLOUD PHYSICS CHANGES

Cloud physics parameters affect the amount of cloud, but we wish to find a combination of effects that increases the amount of moderate optical depth ice cloud and its dependence on rain rate, and also decreases the amount of liquid water cloud in the convective cores. In this section we describe a combination of cloud physics changes that achieves this result.

Another experiment (NOSED) was undertaken in which cloud ice sedimentation is set to zero and the cloud ice to snow autoconversion threshold is lowered from 1.0×10^{-4} kg kg^{-1} to 1.0×10^{-6} kg kg^{-1}. With these changes, the lack of cloud ice sedimentation is offset to some extent by the lower cloud ice autoconversion threshold. This combination of changes is found to produce TOA radiative fluxes closer to observed values in multiscale modeling framework GCM runs than the default SAM settings (M. F. Khairoutdinov 2006, personal communication). Incorporating these changes in another 2D experiment, we find a noticeable increase in the amount of high thin cloud and anvil cloud produced by SAM, and that the relationship between anvil cloud fraction and rain rate varies in a manner similar to the observations (Fig. 5). The amount of high thick cloud becomes excessive at high rain rates, however, as is the case in many of our previous 2D experiments.

To reduce the amount of thick cloud, we set the ice sedimentation to zero and lower the threshold for autoconversion as in NOSED above, but we also increase

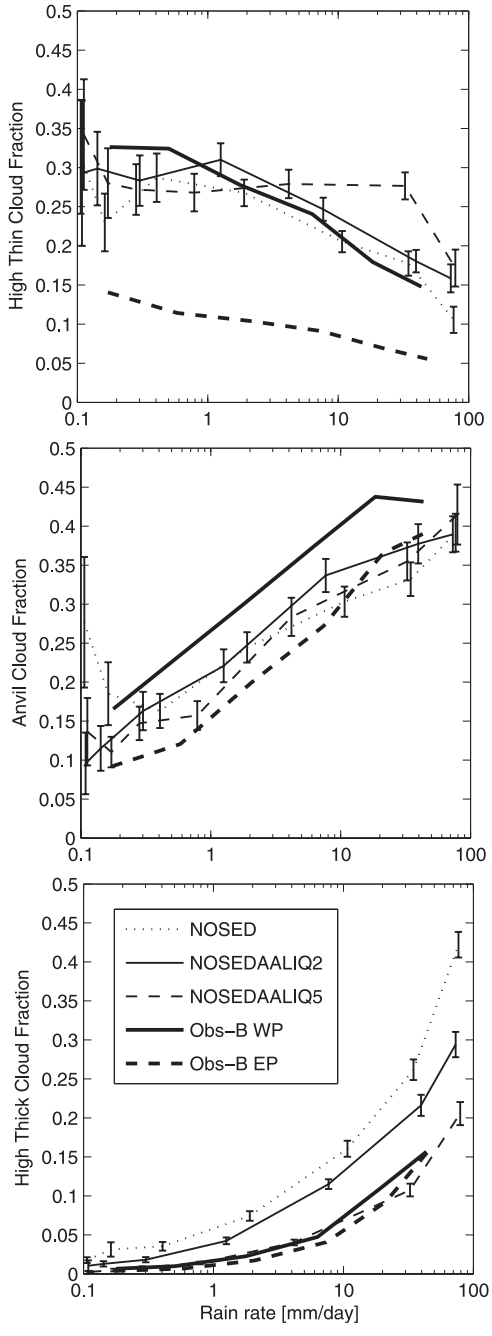

FIG. 5. As in Fig. 2, but the thin lines are for the 2D simulations NOSED, NOSEDAALIQ2, and NOSEDAALIQ5. Heavy lines again represent observations for the EP and WP.

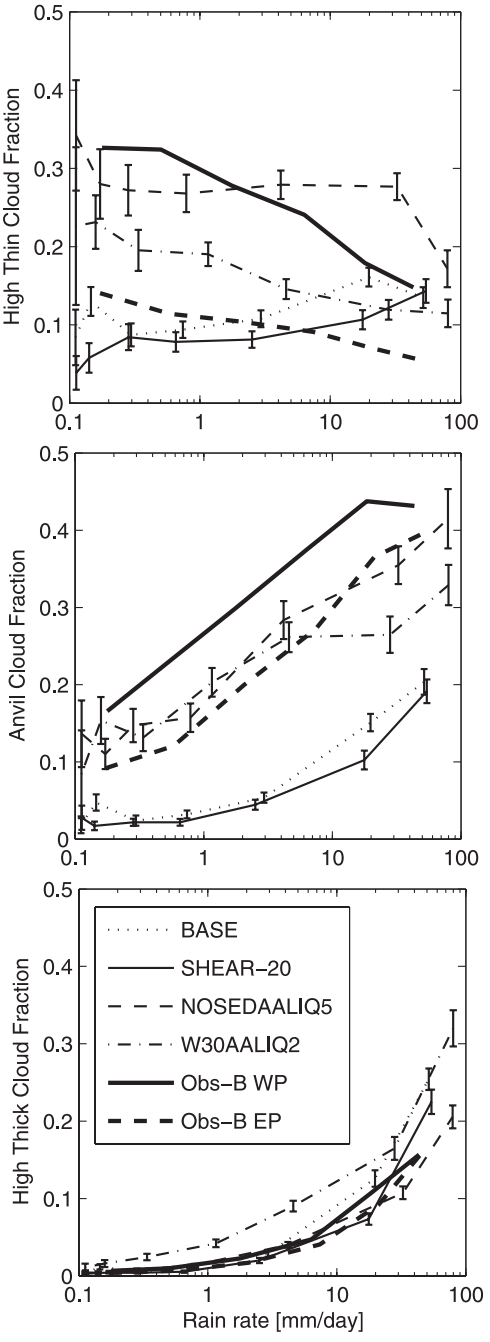

FIG. 6. As in Fig. 2, but the thin lines are for the 2D simulations, BASE, SHEAR-20, NOSEDAALIQ5, and W30AALIQ2.

the rates of autoconversion and accretion for liquid water by factors of 2 and 5 (NOSEDAALIQ2 and NOSEDAALIQ5). The anvil cloud fraction is increased and it has the observed dependence on rain rate as in NOSED, but the amount of thick cloud is also decreased to be much more like the observed amounts, especially for NOSEDAALIQ5 (Fig. 6). We thus have succeeded in tuning the cloud physics parameters to produce a much better simulation of convective cloud optical depth as a function of rain rate. This tuning is not fundamental, as the parameters are not chosen for physical reasons and may be compensating for other errors in the model. Also, it is probable that this tuning is not unique, even within the context of this model. For

example, improved results can also be obtained by limiting the sedimentation velocity in (2) to be no more than 30 cm s^{-1}, and doubling the liquid autoconversion and accretion rate (W30AALIQ2). Both NOSEDAALIQ5 and W30AALIQ2 produce much better simulations of anvil cloud abundances on precipitation rate than the BASE case (Fig. 6).

d. Shear

Many studies have suggested an important role for shear in generating extended upper-level clouds (e.g., Wu 2002; Shie et al. 2003). Lin and Mapes (2004) have used wind and satellite data to examine the relationship of wind shear to tropical clouds and find that shear is associated with changes in OLR of 10–20 W m^{-2}. We test the sensitivity of the modeled clouds to shear by nudging domain mean winds to three different wind profiles. The BASE case in the 2D model is relaxed toward zero domain-mean wind at all levels. We have also done experiments in which the wind decreases from 5 m s^{-1} at the surface to zero at the tropopause (shear 5) and from 5 to -15 m s^{-1} at the tropopause (shear 20). The observed mean wind profiles vary greatly over the course of the seasons in the convective regions of the tropics, but the total wind contrast across the troposphere in the strong shear case is similar to the maximum shears in monthly mean winds, which are observed in the EP region during the months of December–February (DJF). Figure 6 also shows run SHEAR-20, which has the same cloud physics as BASE, but with stronger shear. It can be seen that the cold clouds are slightly reduced, so that strong mean shear does not much influence the abundance of cold clouds when the BASE microphysics is used.

Table 3 shows domain-mean averages for cloud properties for five different 2D experiments to show the relative importance of shear and cloud physical parameters. The BASE cloud physics is compared with W30AALIQ2, and domain-mean shears of 0, 5, and 20 m s^{-2} are considered. First, it can be seen that changing mean shear from 0 to 20 has little effect on the upper-level clouds when the BASE microphysics is used, as already evident from Fig. 6. Changing the microphysics to W30AALIQ2 has a much more significant effect on cold clouds. Because the domain mean surface winds in BASE are 0, changing from BASE to SHEAR-20 increases the mean surface winds, and this increases the amount of low cloud so that stronger shortwave cloud forcing (SWCF) is produced. To remove this effect from a comparison, we do a 2D simulation in which the mean surface wind speed is 5 m s^{-1}, which then decreases to 0 at the tropopause (SHEAR-5). Comparing the last three columns of Table 3 we can see that much of the low-level cloud increase is associated with the increase in surface wind speed between BASE and shear 5 or shear 20. By comparing shear 5 and shear 20, which both have 5 m s^{-1} domain-mean surface wind, we see a substantial increase in cold cloud from 17% to 21%, which is associated with the upper-level shear and not influenced by the surface wind speed. We also see a domain-mean change of OLR and LWCF of about 8 W m^{-2} between case shear 5 and shear 20. This change is similar to the magnitude of tens of watts per meters squared change in OLR with shear observed by Lin and Mapes (2004). Note that the numbers in Table 3 are for the domain mean, which includes both the convective region over the warm water and also the subsiding regions without convective cloud.

e. Microphysical and shear effects in the 3D model

We performed 3D simulations for the WP forcing in which the microphysical parameters from NOSEDAALIQ5 and W30AALIQ2 were employed, as well as different wind shears. In addition, the effect of reducing the imposed thermal forcing to make the model precipitation agree with AMSR is also illustrated. Comparing the first two columns of Table 4 we see that changing from shear 5 to 20 for the BASE cloud physics parameters has a very small effect on the cold cloud abundance, although SWCF is more strongly negative by about 10 W m^{-2} in the strong shear case. Comparing the BASE shear 5 case with the same parameters with a decreased precipitation rate shows that the relative abundance of cold clouds is approximately proportional to rain rate, and the upper-level cloud fractions are much less than observed, even for the strong precipitation rate. Changing to either the NOSEDAALIQ5 or the W30AALIQ2 cloud physics parameters greatly increases the high cloud fraction to more than 50%, even for the weaker forcing, in reasonable agreement with ISCCP observations for the WP region (e.g., Hartmann et al. 1992). In addition, the altered cloud physics gives larger LWCF and SWCF than the BASE cloud physics, and LWCF and SWCF are more similar to each other, as is observed for the WP region. The last column of Fig. 4 shows the effect of using the observed wind profile from TOGA COARE (Wu 2002). This wind profile produces cloud distributions that are similar to those for shear 5 when the W30AALIQ2 cloud physics parameters are used. We conclude from Fig. 6 and Table 4 that shear is not capable of creating realistic anvil clouds, unless we also modify the cloud physics.

7. Conclusions

We have introduced metrics for using satellite data to test the simulation of tropical convection by a cloud-resolving

TABLE 3. Domain-mean parameters for 2D simulations with BASE and W30AALIQ2 cloud physics settings and zero, 5 or 20 m s^{-2} domain-mean shear. Cloud fractions are determined as low ($p > 700$ hPa), mid ($400 < p < 700$ hPa), high ($p < 400$ hPa), and cold ($T_{cloud} < 245$ K).

Run	BASE	BASE shear 20	W30AALIQ2	W30AALIQ2 shear 20	W30AALIQ2 shear 5
Precipitation (mm day^{-1})	3.98	4.12	3.44	3.45	3.41
Cloud cover fraction	0.25	0.40	0.40	0.61	0.51
Precipitable water (mm)	32.10	36.00	32.03	40.78	39.5
Cloud water path (μm)	46.29	63.57	35.86	57.58	50.8
Ice water path (μm)	26.7	28.4	34.4	37.3	34.3
Surface latent heating	113.1	120.1	99.0	99.8	103.5
Heat flux into ocean	63.7	50.8	62.8	57.7	61.1
SWCF (W m^{-2})	−32.8	−53.0	−50.1	−77.5	−65.1
LWCF (W m^{-2})	15.4	20.0	35.8	44.2	37.2
OLR (W m^{-2})	281.8	273.0	261.9	242.7	250.9
Albedo	0.16	0.21	0.20	0.27	0.24
Low cloud fraction	0.10	0.21	0.14	0.26	0.20
Mid cloud fraction	0.07	0.05	0.05	0.04	0.08
High cloud fraction	0.07	0.09	0.19	0.25	0.19
Cold cloud fraction	0.06	0.07	0.17	0.21	0.17

model. Upper-level cloudiness is divided into categories corresponding to the thin cloud, anvil cloud, and deep convective cores that are closely related to precipitation rate. These three categories are chosen to succinctly characterize the relationships among precipitation, cloud structure and the TOA radiation balance in regions of deep convection, and to allow easy comparison with satellite data.

In testing 3D and 2D simulations with the SAM model, we have found that the default model parameters give too little anvil cloud per unit of precipitation, although thin clouds and thick clouds are in much better accord with observations. For the default parameters, anvil clouds are not abundant enough and do not show the observed increase with precipitation rate. The PDFs of OLR and albedo for the default simulation do not show the features that are associated with tropical anvil clouds: a peak in the OLR PDF associated with the anvil cloud-top temperature and a broad distribution of high albedos. Our results are in general agreement with the experiments of Blossey et al. (2007) that attempted to simulate the KWAJEX data.

The amount of cloud ice can easily be increased by decreasing the ice fall speed, but this increases all cold cloud amounts, leading to an overprediction of thin and thick clouds, and so does not improve the ratio of anvil to thick clouds. To produce cloud distributions like those observed, simultaneous changes of several parameters

TABLE 4. Table illustrating the effects of cloud physical parameters, mean shear, and mean rain rate on cloud properties in 3D simulations for WP domain.

Cloud physics	BASE	BASE	BASE	NOSED AALIQ5	W30 AALIQ2	W30 AALIQ2	W30 AALIQ2	W30 AALIQ2
Shear	Shear 5	Shear 20	Shear 5	Shear 5	Shear 5	Shear 20	Shear 5	Shear TC
Forcing			Half-P				Half-P	Half-P
Precipitation (mm day^{-1})	14.65	14.73	9.16	14.58	14.04	14.8	8.32	8.42
Total cloud fraction	0.6	0.64	0.46	89	0.88	0.92	0.77	0.78
Precipitable water (mm)	79.7	84.0	80.2	85.0	83.8	98.1	82.2	85.0
Cloud water path (μm)	95.6	111.9	65.6	38.9	63.5	107.2	42.0	44.9
Ice water path (μm)	88.5	94.2	53.5	82.4	130.4	127.9	78.1	83.2
Snow water path (μm)	53.9	40.4	38.9	35.2	31.5	23.8	20.4	19.3
Heat into ocean (W m^{-2})	102.3	107.4	131	87.3	67.1	88.1	102.3	100.7
SWCF (W m^{-2})	−69.0	−79.3	−48.5	−98.5	−118.9	−137.1	−88.3	−94.0
LWCF (W m^{-2})	48.4	50.1	31.8	93.1	100.7	100.3	77.1	79.0
OLR (W m^{-2})	223.6	221.1	239.7	174.8	168.5	167.5	193.5	191.1
Albedo	0.25	0.27	0.2	0.32	0.37	0.41	0.29	0.31
Low cloud fraction	0.2	0.22	0.15	0.14	0.15	0.23	0.12	0.11
Middle cloud fraction	0.07	0.10	0.04	0.06	0.08	0.23	0.04	0.05
High cloud fraction	0.27	0.29	0.17	0.60	0.69	0.71	0.53	0.56
Cold cloud fraction	0.23	0.24	0.15	0.50	0.58	0.56	0.45	0.45

are necessary. Lowering the ice fall speed increases the amount of anvil cloud and improves its dependence on rain rate, but also increases the amount of thick cloud, so that the ratio of anvil to thick cloud is still imperfect. Adding increased rates of autoconversion and accretion for liquid water to a simulation in which the ice fall speed is reduced gives dependences of thick, anvil, and thin clouds on the rain rate in the 2D model that are in reasonable agreement with observations. The results are not very sensitive to a factor of 4 increase in model resolution. When these changes in cloud physics are introduced, the model shows a response of OLR to mean wind shear that is in accord with observational analysis by Lin and Mapes (2004).

It is unclear to what extent the changes in bulk microphysical parameters used here to produce better simulations are justified on physical grounds, or rather are compensating for other errors in the model microphysics or dynamics. The relative abundance of water and ice in tropical convective clouds is a fundamental issue and deeper understanding of the physical processes whereby ice clouds are formed and maintained is crucial. The physics and dynamics controlling ice amounts in tropical clouds are still uncertain, so that more research is needed to know whether tuning simple cloud schemes like the one used here is an effective strategy for climate modeling, whether more sophisticated cloud physics schemes are needed, and what aspects of current simple bulk models are most in need of improvement. Analysis of observations that allow for the separation of ice and liquid water effects on cloud properties would shed light on the degree to which current models can simulate the correct ratio of ice to liquid water contributions to cloud properties.

Acknowledgments. This work was supported by NSF Grant ATM 04-09075, NASA Grant NNG05GA19G, and NOAA Grant NA06OAR4310055. Marat Khairoutdinhov kindly made SAM available to us at UW. Mark Zelinka provided averaged AIRS profiles for the EP and WP regions and processed reanalysis data for mean wind shear information. Marc Michelsen provided computer expertise.

APPENDIX

Cloud Data versus Precipitation

Binned AMSR precipitation and MODIS cloud-type fractions used in this paper for the selected regions in the tropical EP (7.5°–10°N, 140°–120°W) and WP (5°–7.5°N, 140°–160°E). Data are sorted into six categories of equally probable precipitation rate, and the average cloud fraction for each category is given. Units of precipitation are in millimeters per day. See the text for further details.

	1	2	3	4	5	6
WP precipitation	0.178	0.503	1.77	6.33	18.5	43.4
EP precipitation	0.172	0.582	2.06	7.38	21.1	48.1
WP thin fraction	0.326	0.324	0.278	0.241	0.179	0.148
EP thin fraction	0.141	0.114	0.104	0.0912	0.0700	0.0556
WP anvil fraction	0.166	0.226	0.299	0.375	0.438	0.432
EP anvil fraction	0.0917	0.121	0.200	0.272	0.365	0.394
WP thick fraction	0.00660	0.00978	0.0225	0.0472	0.107	0.157
EP thick fraction	0.00371	0.00681	0.0170	0.0407	0.0922	0.164

REFERENCES

Aumann, H. H., and Coauthors, 2003: AIRS/AMSU/HSB on the aqua mission: Design, science objectives, data products, and processing systems. *IEEE Trans. Geosci. Remote Sens.,* **41,** 253–264.

Back, L. E., and C. S. Bretherton, 2006: Geographic variability in the export of moist static energy and vertical motion profiles in the tropical Pacific. *Geophys. Res. Lett.,* **33,** L17810, doi:10.1029/2006GL026672.

Blossey, P. N., C. S. Bretherton, J. Cetrone, and M. Khairoutdinov, 2007: Cloud-resolving model simulations of KWAJEX: Model sensitivities and comparisons with satellite and radar observations. *J. Atmos. Sci.,* **64,** 1488–1508.

Bony, S., and Coauthors, 2006: How well do we understand and evaluate climate change feedback processes? *J. Climate,* **19,** 3445–3482.

Bretherton, C. S., P. N. Blossey, and M. E. Peters, 2006: Interpretation of simple and cloud-resolving simulations of moist convection-radiation interaction with a mock-Walker circulation. *Theor. Comput. Fluid Dyn.,* **20,** 421–442.

Chen, S. S., R. A. Houze Jr., and B. E. Mapes, 1996: Multiscale variability of deep convection in relation to large-scale circulation in TOGA COARE. *J. Atmos. Sci.,* **53,** 1380–1409.

Chen, T., W. B. Rossow, and Y. C. Zhang, 2000: Radiative effects of cloud-type variations. *J. Climate,* **13,** 264–286.

Comstock, J. M., and C. Jakob, 2004: Evaluation of tropical cirrus cloud properties derived from ECMWF model output and ground based measurements over Nauru Island. *Geophys. Res. Lett.,* **31,** L10106, doi:10.1029/2004GL019539.

DeMoss, J. D., and K. P. Bowman, 2007: Changes in TRMM rainfall due to the orbit boost estimated from buoy rain gauge data. *J. Atmos. Oceanic Technol.,* **24,** 1598–1607.

Donner, L. J., C. J. Seman, R. S. Hemler, and S. M. Fan, 2001: A cumulus parameterization including mass fluxes, convective vertical velocities, and mesoscale effects: Thermodynamic and hydrological aspects in a general circulation model. *J. Climate,* **14,** 3444–3463.

Eitzen, Z. A., and K.-M. Xu, 2005: A statistical comparison of deep convective cloud objects observed by an Earth Observing System satellite and simulated by a cloud-resolving model. *J. Geophys. Res.,* **110,** D15S14, doi:10.1029/2004JD005086.

Fu, Q., and K. N. Liou, 1993: Parameterization of the radiative properties of cirrus clouds. *J. Atmos. Sci.,* **50,** 2008–2025.

——, S. K. Krueger, and K. N. Liou, 1995: Interactions of radiation and convection in simulated tropical cloud clusters. *J. Atmos. Sci.,* **52,** 1310–1328.

Grabowski, W. W., 2001: Coupling cloud processes with the large-scale dynamics using the cloud-resolving convection parameterization (CRCP). *J. Atmos. Sci.,* **58,** 978–997.

——, 2003a: Impact of ice microphysics on multiscale organization of tropical convection in two-dimensional cloud-resolving simulations. *Quart. J. Roy. Meteor. Soc.,* **129,** 67–81.

——, 2003b: MJO-like coherent structures: Sensitivity simulations using the cloud-resolving convection parameterization (CRCP). *J. Atmos. Sci.,* **60,** 847–864.

——, 2003c: Impact of cloud microphysics on convective–radiative quasi equilibrium revealed by cloud-resolving convection parameterization. *J. Climate,* **16,** 3463–3475.

——, J. I. Yano, and M. W. Moncrieff, 2000: Cloud resolving modeling of tropical circulations driven by large-scale SST gradients. *J. Atmos. Sci.,* **57,** 2022–2039.

Hartmann, D. L., H. H. Hendon, and R. A. Houze, 1982: Some implications of the mesoscale circulations in tropical cloud clusters for large-scale dynamics and climate. *J. Atmos. Sci.,* **41,** 113–121.

——, M. E. Ockert-Bell, and M. L. Michelsen, 1992: The effect of cloud type on Earth's energy balance: Global analysis. *J. Climate,* **5,** 1281–1304.

——, L. A. Moy, and Q. Fu, 2001: Tropical convection and the energy balance at the top of the atmosphere. *J. Climate,* **14,** 4495–4511.

Hendon, H. H., and K. Woodberry, 1993: The diurnal cycle of tropical convection. *J. Geophys. Res.,* **98,** 16 623–16 637.

Heymsfield, A. J., 2003: Properties of tropical and midlatitude ice cloud particle ensembles. Part II: Applications for mesoscale and climate models. *J. Atmos. Sci.,* **60,** 2592–2611.

Houze, R. A., 1982: Cloud clusters and large-scale vertical motions in the tropics. *J. Meteor. Soc. Japan,* **60,** 396–410.

Khairoutdinov, M. F., and D. A. Randall, 2003: Cloud resolving modeling of the ARM summer 1997 IOP: Model formulation, results, uncertainties, and sensitivities. *J. Atmos. Sci.,* **60,** 607–625.

Krueger, S. K., Q. A. Fu, K. N. Liou, and H. N. S. Chin, 1995: Improvements of an ice-phase microphysics parameterization for use in numerical simulations of tropical convection. *J. Appl. Meteor.,* **34,** 281–287.

Kubar, T. L., D. L. Hartmann, and R. Wood, 2007: Radiative and convective driving of tropical high clouds. *J. Climate,* **20,** 5510–5526.

Kummerow, C., and Coauthors, 2001: The evolution of the Goddard profiling algorithm (GPROF) for rainfall estimation from passive microwave sensors. *J. Appl. Meteor.,* **40,** 1801–1820.

Lau, K.-M., C.-H. Sui, M.-D. Chou, and W.-K. Tao, 1994: An inquiry into the cirrus-cloud thermostat effect for tropical sea-surface temperature. *Geophys. Res. Lett.,* **21,** 1157–1160.

Leary, C. A., and R. A. Houze, 1980: The contribution of mesoscale motions to the mass and heat fluxes of an intense tropical convective system. *J. Atmos. Sci.,* **37,** 784–796.

Li, J.-L., and B. Mapes, 2004: Wind shear effects on cloud-radiation feedback in the western Pacific warm pool. *Geophys. Res. Lett.,* **31,** L16118, doi:10.1029/2004GL020199.

——, ——, M. H. Zhang, and M. Newman, 2004: Stratiform precipitation, vertical heating profiles, and the Madden–Julian oscillation. *J. Atmos. Sci.,* **61,** 296–309.

——, and Coauthors, 2005: Comparisons of EOS MLS cloud ice measurements with ECMWF analyses and GCM simulations: Initial results. *Geophys. Res. Lett.,* **32,** L18710, doi:10.1029/2005GL023788.

Luo, Y., S. K. Krueger, G. G. Mace, and K.-M. Xu, 2003: Cirrus cloud properties from a cloud-resolving model simulation compared to cloud radar observations. *J. Atmos. Sci.,* **60,** 510–525.

——, ——, and S. Moorthi, 2005: Cloud properties simulated by a single-column model. Part I: Comparison to cloud radar observations of cirrus clouds. *J. Atmos. Sci.,* **62,** 1428–1445.

——, K.-M. Xu, B. A. Wielicki, T. Wong, and Z. A. Eitzen, 2007: Statistical analyses of satellite cloud object data from CERES. Part III: Comparison with cloud-resolving model simulations of tropical convective clouds. *J. Atmos. Sci.,* **64,** 762–785.

Mapes, B. E., and R. A. Houze Jr., 1993: Cloud clusters and superclusters over the oceanic warm pool. *Mon. Wea. Rev.,* **121,** 1398–1416.

——, S. Tulich, J. Lin, and P. Zuidema, 2006: The mesoscale convection life cycle: Building block or prototype for large-scale tropical waves? *Dyn. Atmos. Oceans,* **42,** 3–29.

Miura, H., H. Tomita, T. Nasuno, S. Iga, M. Satoh, and T. Matsuno, 2005: A climate sensitivity test using a global cloud resolving model under an aqua planet condition. *Geophys. Res. Lett.,* **32,** L19717, doi:10.1029/2005GL023672.

Nakazawa, T., 1988: Tropical super clusters within intraseasonal variations over the western Pacific. *J. Meteor. Soc. Japan,* **66,** 823–839.

Ovtchinnikov, M., T. Ackerman, R. Marchand, and M. Khairoutdinov, 2006: Evaluation of the multiscale modeling framework using data from the atmospheric radiation measurement program. *J. Climate,* **19,** 1716–1729.

Pauluis, O., and S. Garner, 2006: Sensitivity of radiative–convective equilibrium simulations to horizontal resolution. *J. Atmos. Sci.,* **63,** 1910–1923.

Platnick, S., M. D. King, S. A. Ackerman, W. P. Menzel, B. A. Baum, J. C. Riedi, and R. A. Frey, 2003: The MODIS cloud products: Algorithms and examples from Terra. *IEEE Trans. Geosci. Remote Sens.,* **41,** 459–473.

Randall, D., M. Khairoutdinov, A. Arakawa, and W. Grabowski, 2003a: Breaking the cloud parameterization deadlock. *Bull. Amer. Meteor. Soc.,* **84,** 1547–1564.

——, and Coauthors, 2003b: Confronting models with data: The GEWEX Cloud Systems Study. *Bull. Amer. Meteor. Soc.,* **84,** 455–469.

Remote Sensing Systems, 2006: Updates to the AMSR-E V05 algorithm. Remote Sensing Systems Tech. Rep. 020706, 5 pp.

Ringer, M. A., and R. P. Allan, 2004: Evaluating climate model simulations of tropical cloud. *Tellus,* **56A,** 308–327.

Rossow, W. B., G. Tselioudis, A. Polak, and C. Jakob, 2005: Tropical climate described as a distribution of weather states indicated by distinct mesoscale cloud property mixtures. *Geophys. Res. Lett.,* **32,** L21812, doi:10.1029/2005GL024584.

Schumacher, C., R. A. Houze, and I. Kraucunas, 2004: The tropical dynamical response to latent heating estimates derived from the TRMM precipitation radar. *J. Atmos. Sci.,* **61,** 1341–1358.

Shie, C. L., W. K. Tao, J. Simpson, and C. H. Sui, 2003: Quasi-equilibrium states in the tropics simulated by a cloud-resolving model. Part I: Specific features and budget analysis. *J. Climate,* **16,** 817–833.

Solomon, S., D. Qin, M. Manning, M. Marquis, K. Averyt, M. M. B. Tignor, H. L. Miller Jr., and Z. Chen, Eds., 2007: *Climate Change 2007: The Physical Science Basis.* Cambridge University Press, 996 pp.

Su, H., C. S. Bretherton, and S. S. Chen, 2000: Self-aggregation and large-scale control of tropical deep convection: A modeling study. *J. Atmos. Sci.,* **57,** 1797–1816.

Tompkins, A. M., and G. C. Craig, 1998: Radiative-convective equilibrium in a three-dimensional cloud-ensemble model. *Quart. J. Roy. Meteor. Soc.,* **124,** 2073–2097.

Wilheit, T., C. D. Kummerow, and R. Ferraro, 2003: Rainfall algorithms for AMSR-E. *IEEE Trans. Geosci. Remote Sens.,* **41,** 204–214.

Wu, X., 2002: Effects of ice microphysics on tropical radiative–convective–oceanic quasi-equilibrium states. *J. Atmos. Sci.,* **59,** 1885–1897.

——, W. D. Hall, W. W. Grabowski, M. W. Moncrieff, W. D. Collins, and J. T. Kiehl, 1999: Long-term behavior of cloud systems in TOGA COARE and their interactions with radiative and surface processes. Part II: Effects of ice microphysics on cloud–radiation interaction. *J. Atmos. Sci.,* **56,** 3177–3195.

Wyant, M. C., C. S. Bretherton, J. T. Bacmeister, J. T. Kiehl, I. M. Held, M. Zhao, S. A. Klein, and B. J. Soden, 2006a: A comparison of low-latitude cloud properties and their response to climate change in three AGCMs sorted into regimes using mid-tropospheric vertical velocity. *Climate Dyn.,* **27,** 261–279.

——, M. Khairoutdinov, and C. S. Bretherton, 2006b: Climate sensitivity and cloud response of a GCM with a superparameterization. *Geophys. Res. Lett.,* **33,** L06714, doi:10.1029/2005GL025464.

Zhou, Y. P., and Coauthors, 2007: Use of high-resolution satellite observations to evaluate cloud and precipitation statistics from cloud-resolving model simulations. Part I: South China Sea Monsoon Experiment. *J. Atmos. Sci.,* **64,** 4309–4329.